Euro. Jnl of Applied Mathematics (2020), *vol.* 31, *pp.* 763–781
doi:10.1017/S0956792519000238

Small Péclet-number mass transport to a finite strip: An advection–diffusion–reaction model of surface-based biosensors†

EHUD YARIV

Department of Mathematics, Technion – Israel Institute of Technology, Haifa 32000, Israel
email: yarivehud@gmail.com

(*Received 30 January 2019*; *revised 15 July 2019*; *accepted 12 August 2019*; *first published online 5 September 2019*)

We consider two-dimensional mass transport to a finite absorbing strip in a uniform shear flow as a model of surface-based biosensors. The quantity of interest is the Sherwood number Sh, namely the dimensionless net flux onto the strip. Considering early-time absorption, it is a function of the Péclet number Pe and the Damköhler number Da, which, respectively, represent the characteristic magnitude of advection and reaction relative to diffusion. With a view towards modelling nanoscale biosensors, we consider the limit $\mathrm{Pe} \ll 1$. This singular limit is handled using matched asymptotic expansions, with an inner region on the scale of the strip, where mass transport is diffusively dominated, and an outer region at distances that scale as $\mathrm{Pe}^{-1/2}$, where advection enters the dominant balance. At the inner region, the mass concentration possesses a point-sink behaviour at large distances, proportional to Sh. A rescaled concentration, normalised using that number, thus possesses a universal logarithmic divergence; its leading-order correction represents a uniform background concentration. At the outer region, where advection by the shear flow enters the leading-order balance, the strip appears as a point singularity. Asymptotic matching with the concentration field in that region provides the Sherwood number as

$$\mathrm{Sh} = \frac{\pi}{\ln(2/\mathrm{Pe}^{1/2}) + 1.0559 + \beta},$$

wherein β is the background concentration. The latter is determined by the solution of the canonical problem governing the rescaled inner concentration, and is accordingly a function of Da alone. Using elliptic-cylinder coordinates, we have obtained an exact solution of the canonical problem, valid for arbitrary values of Da. It is supplemented by approximate solutions for both small and large Da values, representing the respective limits of reaction- and transport-limited conditions.

Key words: advection-diffusion, matched asymptotic expansions, absorption

2010 Mathematics Subject Classification: 35A20; 35A22; 35B25; 35K57; 76R50

1 Introduction

Biomolecular detection and monitoring of analytes in aqueous solutions is a fundamental challenge. In particular, there is a great interest in developing miniaturised label-free surface-based

† This work was supported by the Israel Science Foundation (Grant No. 1081/16).

biosensors on which analytes bind to receptors [9]. The miniaturisation revolution has led to a technological transition from 'microsensors' ($\sim$10 μm length) to 'nanosensors' ($\sim$10 nm length). The latter, implemented by silicon nanowires [5, 4], allow for the rapid detection of small analyte concentrations.

Given the severe time limitations of 'stationary' systems, where the target analytes reach the sensor by pure diffusion [16], it is desirable to employ flowing systems, where forced convection of the analyte-carrying solution significantly enhances collection rate. A paradigmatic system, discussed by Squires *et al.* [17], involves pressure-driven flow between two walls. One of the walls is decorated with a surface-based sensor (say of length $2a$) which is functionalised by a coverage of immobile receptors. The transport of analyte molecules in the solution is described using an advection–diffusion description, while their binding and unbinding to the receptors is modelled using reaction kinetics. The quantity of interest is the net flux of analytes onto the sensor.

The pertinent values characterising realistic systems allow for significant simplifications of the above description. The first has to do with geometry. In many configurations, the sensor width is comparable or even identical to the channel width, which in turn is much larger than other geometric length scales, namely the distance between the walls (the 'channel height') and the length of the sensor. This leads to a convenient two-dimensional (2D) model. The second simplification has to do with disparity of kinetic and diffusive timescales, which allows for a quasi-steady description of the analyte transport in the bulk.

On the continuum level, the absorption of analytes to the sensor gives rise to the formation of a depletion region, about the sensor, where analyte concentration is appreciably reduced. The size and geometry of the depletion region for flowing systems is discussed at length by Squires *et al.* [17], who make a distinction between 'slow' flows, where the depletion region extends upstream of the sensor, and 'fast' flows, where that region is thin compared with channel size. (The distinction is made precise using a Péclet number which is based upon the channel height.) Since the net flux is small in the former case, practical interest lies in the latter, where analyte transport practically occurs under a uniform shear flow – namely the near-wall linear approximation of the parabolic Poiseuille flow.

Focusing upon these fast flows, Squires *et al.* [17] subsequently identified two different régimes, depending upon the sensor size a (or, more precisely, the sensor-based Péclet number, say Pe). The first, corresponding to $\mathrm{Pe} \gg 1$, is where the depletion region thickness is small compared with the sensor length, resulting in narrow boundary-layer structure; the second, corresponding to $\mathrm{Pe} \ll 1$, is where the depletion region is large compared with a. Practically speaking, these two régimes represent analyte transport about micro- and nanosensors, respectively. Motivated by the importance of the latter, we focus here upon the second régime. In what follows, we accordingly address the problem of small Péclet-number mass transport to a finite strip in a uniform shear flow.

Naïvely, it may appear that small Péclet numbers simply imply the neglect of analyte advection. It is well known, however, that the 2D solution of Laplace's equation approaches a source-like behaviour at large distances, which diverges logarithmically. (In the present context, the analyte concentration actually adopts a *sink*-like behaviour, proportional to the net analyte flux onto the sensor.) Such a logarithmic growth is incompatible with the need to approach the uniform equilibrium concentration at large distances away from the sensor. That incompatibility

https://doi.org/10.1017/S0956792519000238 Published online by Cambridge University Press

is a manifestation of the well-known singular nature of the small Péclet-number limit [12], where the associated approximation of diffusive transport breaks down at large distances. (While that singularity appears in both 2D and 3D problems, it is more acute in the former.) It is remedied by the use of matched asymptotic expansions [8], whereby the transport domain is conceptually decomposed into two regions: an 'inner' region at the neighbourhood of the sensor, where the assumption of diffusive transport applies, and an 'outer' region at large distances, where advection enters the leading-order balance. In the 2D context, the small Péclet-number singularity has been originally confronted in the classical problem of heat transport from a cylinder in a uniform shear flow [3, 7]. (See Ref. [19] for a more general discussion.) Similar asymptotic methods will be used here to investigate the small Péclet-number limit in the context of surface-based sensors.

In describing analyte absorption, we seek to employ an approximate yet reasonable kinetic model. We accordingly focus upon the early stages of the absorption process, where the concentration of the bound receptors is small. This results in a simple kinetic description, wherein the diffusive flux of analytes into the sensor is proportional to their surface concentration. (Similar descriptions have been extensively used in modelling chemically active colloids [6, 13, 21].) The resulting decoupling of the analyte-transport problem from the time evolution of the bound-receptors concentration constitutes a significant simplification: indeed, the associated dimensionless problem depends only upon two parameters, namely the Damköhler number Da, representing the ratio of diffusive-to-reactive timescales, and the Péclet number Pe, representing the ratio of diffusive-to-advective timescales.

The closest relevant analysis in the literature is that of Ackerberg *et al.* [1], who considered heat transport to an isothermal strip. That analysis may be adapted to the comparable mass-transport problem provided one (i) considers early times, as above, where the concentration of the bound receptors is small, and (ii) assumes transport-limited conditions, $\mathrm{Da} \to \infty$, when reaction is fast compared with diffusion. As noted by Squires *et al.* [17], however, the Damköhler number is actually *small* for typical kinetic parameters pertaining to nanowire sensors. (This is hardly surprising, since that number is proportional to the strip length; see equation (3.2).) We accordingly consider here the general case of an arbitrary value of Da (expecting our results to degenerate to those of Ref. [1] at large values of that number), with a particular interest in small Damköhler numbers.

Experimental observations of analyte absorption at nanowire sensors differ from theoretical estimates by orders of magnitudes [18, 22]. These discrepancies motivate the need for a careful analysis of the associated absorption processes [17]. Our asymptotic analysis, which incorporates a reasonable model of chemical kinetics, is a first step in that direction.

2 Physicochemical problem

The 2D transport problem considered herein involves a semi-bounded liquid domain which is in contact with a planar solid wall; see Figure 1. The liquid contains analyte molecules of an otherwise uniform volumetric concentration, say $\mathcal{A}$. It undergoes a uniform shear flow (shear-rate G). Our interest is in the analyte-transport process that occurs due to the introduction of a reactive strip, say of length $2a$, at the chemically inert wall. In particular, we assume that the strip is covered with immobile receptors, say with a uniform areal concentration $\mathcal{R}$. Analyte transport

https://doi.org/10.1017/S0956792519000238 Published online by Cambridge University Press

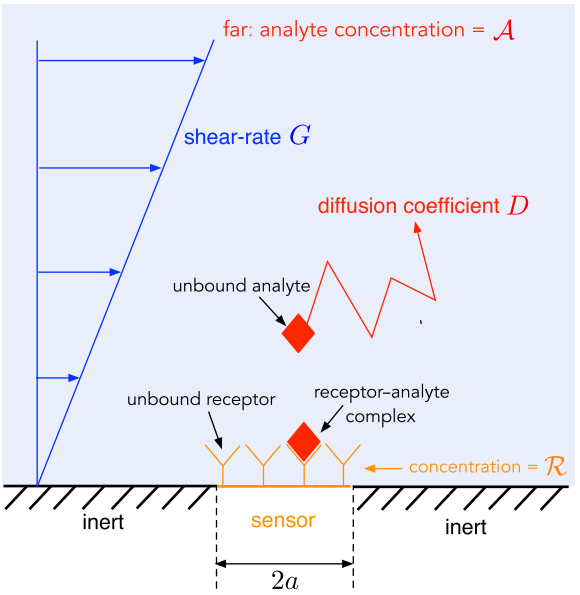

FIGURE 1. Schematic.

to the strip takes place by both Brownian motion (represented by molecular diffusivity D) and advection by the shear flow. Our ultimate interest is in the net transport of analytes onto the strip.

The chemical reaction at the strip is represented by the binding of receptor (R) and analyte (A) molecules to form receptor–analyte (RA) complexes, and the unbinding of these complexes. These transformations are modelled using the standard receptor–ligand kinetics

$$\mathrm{R} + \mathrm{A} \rightleftharpoons \mathrm{RA}. \tag{2.1}$$

On the continuum level, these are described in terms of the volumetric concentration [A] of unbound analytes as well as the respective areal concentrations [R] and [RA] of unbound and bound receptors. The forward binding transition $\mathrm{R} + \mathrm{A} \to \mathrm{RA}$ is characterised by the on-rate constant k_{on} while the backward unbinding transition $\mathrm{RA} \to \mathrm{R} + \mathrm{A}$ is characterised by the off-rate constant k_{off}. The receptor–ligand transformations (2.1) are accordingly manifested by Langmuir kinetics,

$$\text{time derivative of } [\mathrm{RA}] = k_{\mathrm{on}}[\mathrm{R}][\mathrm{A}] - k_{\mathrm{off}}[\mathrm{RA}], \tag{2.2}$$

at any point along the strip. Note that (i) the left-hand side of (2.2) is equal to the diffusive flux of analytes from the bulk; (ii) with $[\mathrm{R}] + [\mathrm{RA}] = \mathcal{R}$, the maximum possible value of [RA] is $\mathcal{R}$; (iii) at equilibrium, the ratio of bound to unbound receptors is $[\mathrm{RA}]/[\mathrm{R}] = [\mathrm{A}]/K_D$, wherein $K_D = k_{\mathrm{off}}/k_{\mathrm{on}}$ is the dissociation constant; and (iv) the balance (2.2) provides the reactive timescale

$$\tau_{\mathrm{R}} = \frac{1}{k_{\mathrm{on}}\mathcal{A}}. \tag{2.3}$$

https://doi.org/10.1017/S0956792519000238 Published online by Cambridge University Press

3 Problem formulation

3.1 Dimensionless formulation

We employ a dimensionless notation where length variables are normalised by a and the time t by τ_R. The dimensionless analyte and bound-receptor concentrations are defined as $c = [A]/\mathcal{A}$ and $b = [RA]/\mathcal{R}$, respectively. The dimensionless problem involves four parameters. These are the Péclet number,

$$\mathrm{Pe} = \frac{a^2 G}{D}, \tag{3.1}$$

which represents the ratio of advection to diffusion; the Damköhler number

$$\mathrm{Da} = \frac{a k_{on} \mathcal{R}}{D}, \tag{3.2}$$

which represents the ratio of reaction to diffusion; the concentration ratio $\mathcal{C} = \mathcal{A}/K_D$, which indicates how 'dilute' is the solution; and the timescale ratio $\Lambda = \tau_D/\tau_R$, wherein $\tau_D = a^2/D$ is the diffusive scale.

We make use of the (x, y) Cartesian coordinates, where the x-axis, which points in the flow direction, coincides with the solid wall, and the y-axis points into the liquid. The origin is chosen in the centre of the strip. The analyte concentration $c(x, y, t)$ is governed by (i) the conservation equation,

$$\Lambda \frac{\partial c}{\partial t} + \mathrm{Pe}\, y \frac{\partial c}{\partial x} = \nabla^2 c \quad \text{for} \quad y > 0; \tag{3.3}$$

(ii) the no-flux condition at the inert portions of the wall,

$$\frac{\partial c}{\partial y} = 0 \quad \text{at} \quad y = 0 \quad \text{for} \quad |x| > 1; \tag{3.4}$$

(iii) the kinetic condition [cf. (2.2)],

$$\frac{\partial c}{\partial y} = \mathrm{Da}\ \{c(1 - b) - b/\mathcal{C}\} \quad \text{at} \quad y = 0 \quad \text{for} \quad |x| < 1; \tag{3.5}$$

and (iv) the approach to a unity analyte concentration at large distances,

$$c \to 1 \quad \text{for} \quad r \to \infty, \tag{3.6}$$

wherein $r = \sqrt{x^2 + y^2}$.

The preceding problem is coupled to the bound-receptor concentration $b(x, t)$, which is governed by the following evolution equation:

$$\frac{\partial b}{\partial t} = c(1 - b) - b/\mathcal{C} \quad \text{for} \quad -1 < x < 1, \tag{3.7}$$

where c is evaluated at $y = 0$. The latter equation introduces an explicit time dependence, which necessitates the introduction of appropriate initial conditions. These are given by

$$c \equiv 1, \quad b \equiv 0 \tag{3.8a, b}$$

https://doi.org/10.1017/S0956792519000238 Published online by Cambridge University Press

at $t = 0$. Thus, the above formulation faithfully represents the unsteady process which results when an initially homogenous solution is brought into contact with a sensor-supporting wall and is exposed to a uniform shear flow.

Our goal is the Sherwood number (also called the mass-transfer Nusselt number), namely the net analyte flux onto the strip (normalised by $\mathcal{A}D$):

$$\mathrm{Sh} = \int_{-1}^{1} \left.\frac{\partial c}{\partial y}\right|_{y=0} dx. \tag{3.9}$$

It is a function of t and the above-mentioned parameters.

3.2 Simplified problem

In virtually all practical problems, the diffusive timescale is much shorter than the reactive one [17], whereby $\Lambda \to 0$. The conservation equation (3.3) is then replaced by the quasi-steady advection–diffusion equation

$$\nabla^2 c = \mathrm{Pe}\, y \frac{\partial c}{\partial x} \quad \text{for} \quad y > 0. \tag{3.10}$$

In what follows, we focus here upon early times, where the concentration of bound receptors is small, $b \ll 1$. In these times, condition (3.5) is simplified to

$$\frac{\partial c}{\partial y} = \mathrm{Da}\, c \quad \text{at} \quad y = 0 \quad \text{for} \quad |x| < 1. \tag{3.11}$$

The coupling with b, which has entered through (3.5), disappears, as does the dependence upon $\mathcal{C}$. More importantly, with the evolution equation (3.7) being irrelevant, there is no time dependence in the problem, explicit or implicit. Consistently, the initial condition (3.8*a*) is abandoned. We accordingly denote hereafter the analyte concentration by $c(x, y)$. The (misleadingly simple looking) problem governing that field is conveniently summarised in Figure 2. Note that the Sherwood number (3.9) is now a function of Pe and Da alone.

3.3 Small Péclet numbers

Our interest is in the limit of small Péclet numbers, $\mathrm{Pe} \ll 1$, representing analyte transport about nanosensors. Naïvely, it may appear that at leading order the advection–diffusion equation (3.10) simply degenerates to Laplace's equation. In the present context, however, it is impossible to find a 2D solution of Laplace's equation that approaches a uniform value at infinity, as specified by condition (3.6). The reason has to do with the net flux into the strip: at large distances the strip appears like a point sink, implying a logarithmic variation with r of c.

The singularity of the small-Pe limit is handled using matched asymptotic expansions. Thus, we conceptually decompose the liquid domain into an inner region at the scale of the strip, $r = O(1)$, where c is dominated by diffusion, and an outer region at large distances, where analyte advection and diffusion are comparable.

https://doi.org/10.1017/S0956792519000238 Published online by Cambridge University Press

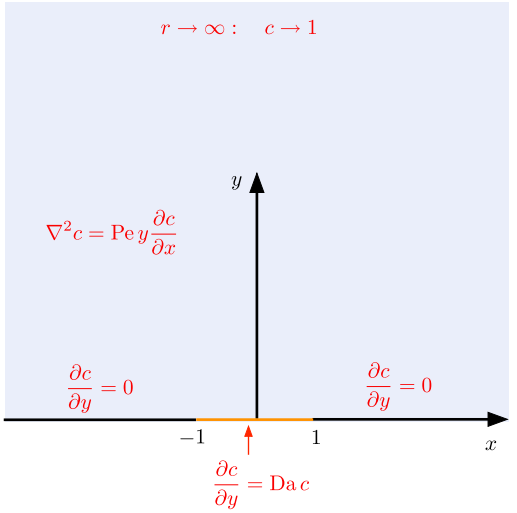

FIGURE 2. Simplified dimensionless problem.

4 Inner region

Consider first the leading-order inner problem, consisting of Laplace's equation governing c and the boundary conditions (3.4) and (3.11) at $y = 0$ (see Figure 2). Condition (3.6) does not apply in the inner region. Rather, c must behave as $\ln r$ at large r. More specifically, consistency with definition (3.9) implies that

$$c \sim \frac{\mathrm{Sh}}{\pi} \ln r \quad \text{for} \quad r \to \infty. \tag{4.1}$$

Since the only inhomogeneity in the inner problem enters through (4.1), it follows that c is linear and homogeneous in Sh. We therefore write

$$c(x, y) = \mathrm{Sh}\, \tilde{c}(x, y). \tag{4.2}$$

The rescaled concentration $\tilde{c}$ is independent of Sh. It satisfies the following: (i) Laplace's equation,

$$\nabla^2 \tilde{c} = 0; \tag{4.3}$$

(ii) the boundary conditions at $y = 0$,

$$\frac{\partial \tilde{c}}{\partial y} = 0 \quad \text{for} \quad |x| > 1, \qquad \frac{\partial \tilde{c}}{\partial y} = \mathrm{Da}\, \tilde{c} \quad \text{for} \quad |x| < 1; \tag{4.4a, b}$$

and (iii) the universal behaviour [cf. (4.1)]

$$\tilde{c} \sim \frac{1}{\pi} \ln r \quad \text{for} \quad r \to \infty. \tag{4.5}$$

Conditions (4.4) and (4.5) serve to uniquely define the harmonic function $\tilde{c}$. The canonical problem governing $\tilde{c}$ depends only upon the single parameter Da. The dependence of the unscaled

https://doi.org/10.1017/S0956792519000238 Published online by Cambridge University Press

inner field c upon the Péclet number enters only through the dependence of Sh upon that number. As we shall see in the following, the latter dependence is provided by the requirement of asymptotic matching.

At this point, we make the following observations. First, since matching with the outer solution is expressed in the canonical problem through the *isotropic* condition (4.5), it is evident that $\tilde{c}$ is symmetric with respect to x:

$$\tilde{c}(-x, y) = \tilde{c}(x, y). \tag{4.6}$$

(This symmetry does not necessarily hold at higher asymptotic orders.)

Second, note that (3.9) in conjunction with (4.2) implies that

$$\int_{-1}^{1} \frac{\partial \tilde{c}}{\partial y}(x, 0)\, dx = 1. \tag{4.7}$$

[This could have been alternatively obtained using (4.5) in conjunction with the 2D variant of Gauss's theorem.] Condition (4.4*b*) then imposes the constraint

$$\mathrm{Da} \int_{-1}^{1} \tilde{c}(x, 0)\, dx = 1. \tag{4.8}$$

Since constraints (4.7) and (4.8) follow from the problem formulation, they do not provide independent information. Nonetheless, they prove useful in the asymptotic analysis that follows.

Last, the large-r asymptotic behaviour (4.5) constitutes the leading term in an asymptotic series. In particular, the correction term to (4.5) is a constant, representing a 'background' concentration, while subsequent terms decay algebraically fast at large r. We accordingly write

$$\pi \tilde{c} \sim \ln(2r) + \beta + \cdots \quad \text{for} \quad r \gg 1, \tag{4.9}$$

where the 2-factor is introduced for convenience and the asymptotic error is 'algebraically small' (i.e. smaller than some positive power of $1/r$). The background concentration β is determined by the solution of the canonical problem; consequently, it is a function of the single parameter Da.

5 Outer problem and asymptotic matching

It follows from (3.10) that a small-Pe balance between advection and diffusion takes place when

$$r = O(\mathrm{Pe}^{-1/2}). \tag{5.1}$$

We accordingly define the outer Cartesian coordinates $(X, Y) = \mathrm{Pe}^{1/2}(x, y)$ and the corresponding radial coordinate $R = \mathrm{Pe}^{1/2} r$. In the outer region, where $R = O(1)$, the strip appears like a point singularity at the origin.

5.1 Outer problem

Consider now the outer-region concentration, denoted by $C(X, Y)$. It is governed by the advection–diffusion equation [cf. (3.10)],

$$\frac{\partial^2 C}{\partial X^2} + \frac{\partial^2 C}{\partial Y^2} = Y \frac{\partial C}{\partial X} \quad \text{for} \quad Y > 0; \tag{5.2}$$

https://doi.org/10.1017/S0956792519000238 Published online by Cambridge University Press

the no-flux condition [cf. (3.4)],

$$\frac{\partial C}{\partial Y} = 0 \quad \text{at} \quad Y = 0 \quad \text{for} \quad |X| \neq 0; \tag{5.3}$$

and the approach to the equilibrium value [cf. (3.6)]

$$C \to 1 \quad \text{for} \quad R \to \infty. \tag{5.4}$$

The limit $\mathrm{Pe} \ll 1$ may be interpreted as that corresponding to a strip of shrinking size. Since a vanishingly small strip can have no effect on the analyte concentration, it is evident from (5.4) that at leading order $C \equiv 1$. Asymptotic matching with (4.1) then suggests that $C - 1$ is of the order Sh (implying, *inter alia*, that $\mathrm{Sh} \ll 1$). We accordingly write

$$C = 1 + \mathrm{Sh}\,\tilde{C}. \tag{5.5}$$

At leading order $\tilde{C}$ satisfies (5.2) and (5.3), large-R decay and the requirement of asymptotic matching with (4.1), namely

$$\tilde{C} \sim \frac{1}{\pi} \ln R \quad \text{for} \quad R \ll 1. \tag{5.6}$$

This matching condition, in conjunction with (5.3), gives

$$\frac{\partial \tilde{C}}{\partial Y} = \delta(X) \quad \text{at} \quad Y = 0. \tag{5.7}$$

5.2 Fourier-transform solution

The problem governing $\tilde{C}$ is identical to that appearing in Ref. [1] (provided that their variable k is set to unity). This was to be expected, since the different transport mechanism at the inner region does not affect the universal growth (4.1). The matching process we employ here is simpler than that of Ref. [1]. We accordingly we find it convenient to describe the calculation of $\tilde{C}$.

We employ the Fourier transform and its inverse,

$$\hat{C}(\alpha, Y) = \int_{-\infty}^{\infty} \tilde{C}(X, Y) e^{i\alpha X}\, dX, \tag{5.8a}$$

$$\tilde{C}(X, Y) = \frac{1}{2\pi} \int_{-\infty}^{\infty} \hat{C}(\alpha, Y) e^{-i\alpha X}\, d\alpha. \tag{5.8b}$$

Forming the transform of (5.2) yields the Airy equation

$$\frac{d^2 \hat{C}}{d\zeta^2} - \zeta \hat{C} = 0, \tag{5.9}$$

wherein

$$\zeta = e^{-i\pi/6} \alpha^{1/3} (Y + i\alpha). \tag{5.10}$$

The solution of (5.9) which decays at large R is

$$\hat{C} = H(\alpha)\, \mathrm{Ai}(\zeta), \tag{5.11}$$

https://doi.org/10.1017/S0956792519000238 Published online by Cambridge University Press

where the requirement $|\arg\zeta| < \pi/3$ implies that

$$-\pi/2 < \arg\alpha < 3\pi/2. \tag{5.12}$$

A branch cut, which extends along the negative imaginary axis, is accordingly introduced in the complex α-plane. Forming the transform of (5.7) gives $H(\alpha) = e^{i\pi/6}/\alpha^{1/3}\,\mathrm{Ai}'(\zeta_0)$, wherein

$$\zeta_0 = \zeta|_{Y=0} = e^{i\pi/3}\alpha^{4/3} \tag{5.13}$$

and the prime denotes differentiation with respect to the argument. The inversion formula (5.8*b*) then gives

$$\tilde{C}(X,Y) = \frac{1}{2\pi}\int_{-\infty}^{\infty} \frac{e^{i\pi/6}\,\mathrm{Ai}(\zeta)}{\alpha^{1/3}\,\mathrm{Ai}'(\zeta_0)} e^{-i\alpha X}\,d\alpha. \tag{5.14}$$

5.3 Asymptotic matching

Towards asymptotic matching with the inner region, we now restrict the attention to $Y = 0$, whereby $\zeta = \zeta_0$. The outer concentration (5.14) becomes

$$\tilde{C}(X,0) = \frac{1}{2\pi}\int_{-\infty}^{\infty} \frac{e^{i\pi/6}\,\mathrm{Ai}(\zeta_0)}{\alpha^{1/3}\,\mathrm{Ai}'(\zeta_0)} e^{-i\alpha X}\,d\alpha. \tag{5.15}$$

Since all the zeros of $\mathrm{Ai}'(\zeta_0)$ are located on the negative real axis of the complex ζ_0-plane, the isolated singularities of the integrand are located at the positive imaginary axis of the complex α-plane. For $X < 0$, where $e^{-\alpha X}$ decays at large and positive $\mathrm{Im}\,\alpha$, the integral (5.15) is evaluated by forming a closed contour in the upper half-plane of the complex α-plane and making use of Cauchy's residue theorem, thereby providing $\tilde{C}(X,0)$ as an infinite series. For $X > 0$, on the other hand, the integration interval is conveniently represented as the union of two semi-infinite sub-intervals, one from $-\infty$ to 0 and one from 0 to ∞. Since here $e^{-\alpha X}$ decays at large and negative $\mathrm{Im}\,\alpha$, and with the integrand having no singularities in the lower half α-plane, these sub-intervals may be, respectively, replaced by two rays, proximate to the branch cut, at $\alpha = 0^-$ and $\alpha = 0^+$. Consistently with (5.12), the parameterisation of α along these rays is, respectively, given by $\alpha = se^{3i\pi/2}$ and $\alpha = se^{-i\pi/2}$, where the real parameter s extends between zero and infinity. We then obtain

$$\tilde{C}(X,0) = \frac{1}{\pi}\,\mathrm{Re}\left\{I(X)\right\}, \tag{5.16}$$

wherein

$$I(X) = \int_0^{\infty} \frac{e^{-i\pi/6}\,\mathrm{Ai}(e^{-i\pi/3}s^{4/3})}{s^{1/3}\,\mathrm{Ai}'(e^{-i\pi/3}s^{4/3})} e^{-sX}\,ds. \tag{5.17}$$

The difference in the type of expressions which apply for negative and positive X has to do with (5.2) which, unlike (4.3), is *asymmetric* with respect to X.

In what follows, we only need the positive-X expression (5.16). In Appendix A, we show that (5.16) and (5.17) give

$$\pi\tilde{C}(X,0) \sim \ln X - \lambda + o(1) \quad \text{for} \quad 0 < X \ll 1, \tag{5.18}$$

https://doi.org/10.1017/S0956792519000238 Published online by Cambridge University Press

wherein

$$\lambda = 1.0559 \tag{5.19}$$

and the asymptotic error is algebraically small. This approximation agrees with the one obtained in Ref. [1].

In performing the asymptotic matching, we follow van Dyke's convention, considering logarithmically small terms on par with $O(1)$ terms [8, 20]. Comparing (5.5) and (5.18) with (4.2) and (4.9), the latter evaluated at $y = 0$ and $x > 0$, we readily obtain

$$\mathrm{Sh} = \frac{\pi}{\ln(2/\mathrm{Pe}^{1/2}) + \lambda + \beta(\mathrm{Da})}, \tag{5.20}$$

which is indeed $\ll 1$ in the small Péclet-number limit, as required.

The Sherwood number is affected by the inner-region transport only through the value of the background concentration β. When β increases, the 'difference' between the analyte-concentration value at the 'outer edge' of the inner region and the unity value at infinity is curtailed, resulting in a smaller diffusive flux from infinity. It is therefore unsurprising that the overall flux, as provided by the Sherwood number, decreases.

Expression (5.20) constitutes our key result. As indicated in (5.20), the dependence upon Da enters only through the dependence of β upon that parameter. In what follows, we evaluate that dependence by solving the canonical inner problem.

6 Solution of the canonical problem

The canonical problem in the semi-bounded geometry $y > 0$ is naturally handled using elliptic-cylinder coordinates [14]; see Figure 3. The constant-η curves are the ellipses

$$\frac{x^2}{\cosh^2\eta} + \frac{y^2}{\sinh^2\eta} = 1, \tag{6.1}$$

while the constant-ψ curves are the hyperboles

$$\frac{x^2}{\cos^2\psi} - \frac{y^2}{\sin^2\psi} = 1. \tag{6.2}$$

In terms of these coordinates, the upper-half plane $y > 0$ is covered by $\eta > 0$ and $0 < \psi < \pi$, while the strip is the line segment $\eta = 0$. Note that

$$\eta \sim \ln(2r) + o(1) \quad \text{for} \quad r \gg 1, \tag{6.3}$$

and that, at the strip, $x = \cos\psi$. Making use of the transformation

$$\left.\frac{\partial}{\partial y}\right|_{y=0,-1<x<1} = \frac{1}{\sin\psi}\left.\frac{\partial}{\partial\eta}\right|_{\eta=0}, \tag{6.4}$$

https://doi.org/10.1017/S0956792519000238 Published online by Cambridge University Press

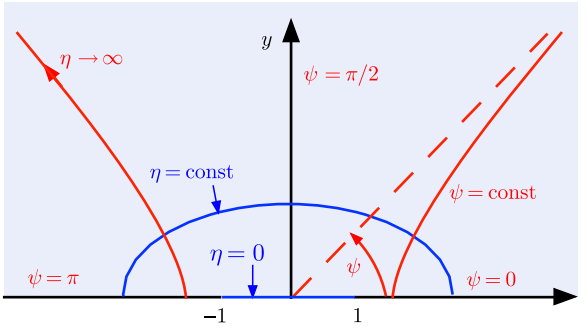

FIGURE 3. Elliptic-cylinder coordinates.

we find that constraints (4.7) and (4.8), respectively, read

$$\int_0^{\pi} \left.\frac{\partial \tilde{c}}{\partial \eta}\right|_{\eta=0} d\psi = 1, \tag{6.5a}$$

$$\mathrm{Da} \int_0^{\pi} \tilde{c}|_{\eta=0} \sin\psi \, d\psi = 1. \tag{6.5b}$$

6.1 Exact solution

To determine $\tilde{c}(\eta, \psi)$, we note that Laplace's equation (4.3) remains invariant when expressed in terms of the elliptic-cylinder coordinates,

$$\frac{\partial^2 \tilde{c}}{\partial \eta^2} + \frac{\partial^2 \tilde{c}}{\partial \psi^2} = 0 \quad \text{for} \quad \eta > 0, \quad 0 < \psi < \pi; \tag{6.6}$$

while condition (4.4a) reads

$$\frac{\partial \tilde{c}}{\partial \psi} = 0 \quad \text{for} \quad \psi = 0, \pi. \tag{6.7}$$

We accordingly seek a solution of (6.6) which is an even function of $\psi - \pi/2$ [see (4.6)] and satisfies both (4.5) and (6.7). Using separation of variables and noting (6.3), we readily obtain the Fourier-series solution,

$$\pi \tilde{c} = \eta + \sum_{n=0}^{\infty} A_n e^{-2n\eta} \cos 2n\psi. \tag{6.8}$$

The coefficients $\{A_n\}_{n=0}^{\infty}$ are determined using condition (4.4b), which here reads [see (6.4)]

$$\frac{\partial \tilde{c}}{\partial \eta} = \mathrm{Da}\, \tilde{c} \sin\psi \quad \text{for} \quad \eta = 0. \tag{6.9}$$

Upon substitution of (6.8), we therefore obtain

$$1 - 2\sum_{n=0}^{\infty} n A_n \cos 2n\psi = \mathrm{Da} \sum_{n=0}^{\infty} A_n \cos 2n\psi \sin\psi. \tag{6.10}$$

https://doi.org/10.1017/S0956792519000238 Published online by Cambridge University Press

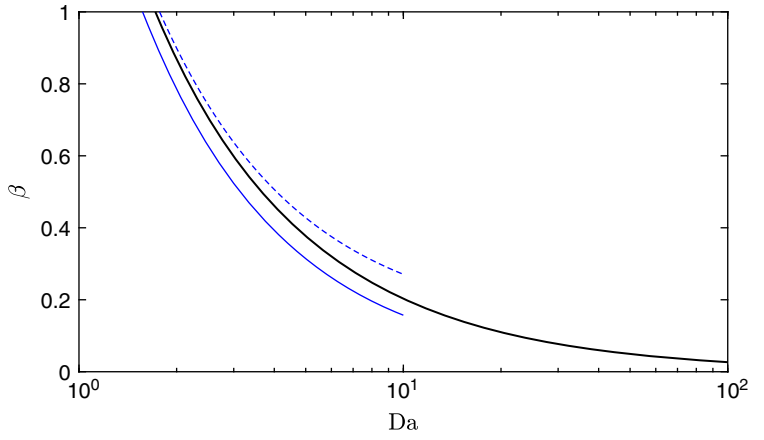

FIGURE 4. Variation of β with Da. Solid: exact solution, as obtained from (6.11) and (6.13). Thin: one-term small-Da approximation (6.20). Dashed: two-term small-Da approximation (6.21).

Multiplying by $\cos 2m\psi$ $(m = 0, 1, \ldots)$ and integrating over the interval $(0, \pi/2)$ yields the equation

$$2\mathrm{Da}\sum_{n=0}^{\infty} F_{mn}A_n + \pi m A_m = \pi\delta_{m0}, \quad m = 0, 1, \ldots, \tag{6.11}$$

wherein

$$F_{mn} = \frac{1 - 4m^2 - 4n^2}{16m^4 - 8m^2\left(4n^2 + 1\right) + \left(4n^2 - 1\right)^2}. \tag{6.12}$$

The infinite linear system governing $\{A_m\}_{m=0}^{\infty}$ is readily solved by controlled truncation. Once these coefficients are determined, the value of β is obtained. Thus, comparing (4.9) with (6.3) and (6.8), we find that

$$\beta = A_0. \tag{6.13}$$

The universal function $\beta(\mathrm{Da})$ is presented in Figure 4. The monotonic decrease of β with Da is expected: the stronger is the reaction, the lower is the 'mean' value of the analyte concentration at the 'surroundings' of the strip (namely the outer edge of the inner region).

6.2 Approximate solutions for Da $\gg$ 1

In addition to the exact solution of the canonical problem for arbitrary Da, it is desirable to obtain approximate expressions for $\beta(\mathrm{Da})$ in the diametric limits $\mathrm{Da} \ll 1$ and $\mathrm{Da} \gg 1$. Consider first the transport-limited case $\mathrm{Da} \gg 1$. From (6.5), we find that, at $\eta = 0$, $\partial\tilde{c}/\partial\eta = O(1)$ while $\tilde{c} = O(\mathrm{Da}^{-1})$. Comparing with the Fourier-series representation (6.8), we find that these two apparently contradictory balances are satisfied if, at leading order, we retain the first term in (6.8) while setting $A_n = 0$ for all n. This gives

$$\tilde{c} = \eta/\pi + o(1). \tag{6.14}$$

https://doi.org/10.1017/S0956792519000238 Published online by Cambridge University Press

With β vanishing at $O(1)$, we conclude that

$$\lim_{\mathrm{Da}\to\infty} \beta = 0, \tag{6.15}$$

as is indeed apparent in Figure 4. This minimal value of β is expected at large Damköhler numbers, where the reaction is fast enough to eliminate the background analyte concentration. The leading term in (6.14) coincides with the solution obtained in Ref. [1] using conformal mapping, namely

$$\frac{1}{\pi}\,\mathrm{Re}\left\{\log[z+(z^2-1)^{1/2}]\right\}, \tag{6.16}$$

wherein $z = x + iy$. This was to be expected: as explained in Section 1, the problem formulation in Ref. [1] corresponds to the large-Da limit of the early-time evolution considered herein.

6.3 Approximate solution for Da $\ll$ 1

Consider now the reaction-limited régime, Da $\ll 1$, where equations (4.7) and (4.8) suggest that $\tilde{c} = O(\mathrm{Da}^{-1})$ while $\partial\tilde{c}/\partial y = O(1)$. As these scalings allow for a uniform $O(\mathrm{Da}^{-1})$ term in $\tilde{c}$, we postulate the expansion

$$\tilde{c} = \frac{\beta_{-1}}{\pi\,\mathrm{Da}} + \tilde{c}_0(x,y) + \cdots, \tag{6.17}$$

in which the leading $O(\mathrm{Da}^{-1})$ uniform term trivially satisfies Laplace's equation (4.3) and the homogeneous Neumann condition (4.4*a*). The requisite value β_{-1} is determined from the solvability conditions at the next asymptotic order. Thus, we make use of the $O(1)$ balance of (4.4*b*),

$$\frac{\partial\tilde{c}_0}{\partial y} = \frac{\beta_{-1}}{\pi} \quad \text{at} \quad y = 0 \quad \text{for} \quad |x| < 1, \tag{6.18}$$

which, when substituted into (4.7), gives

$$\beta_{-1} = \pi/2. \tag{6.19}$$

We conclude that

$$\beta \sim \frac{\pi}{2\mathrm{Da}} \quad \text{for} \quad \mathrm{Da} \ll 1. \tag{6.20}$$

An improved two-term approximation,

$$\beta \sim \frac{\pi}{2\mathrm{Da}} + \frac{3}{2} - \ln 4 + o(1) \quad \text{for} \quad \mathrm{Da} \ll 1, \tag{6.21}$$

is derived in Appendix B. A comparison between the above approximations and the exact solution is illustrated in Figure 4. When using (6.21), an excellent agreement is observed even for Da-values larger than one.

A curious feature of approximation (6.20) is that, on a rough scale, it appears to be indistinguishable from the exact variation. This is a mere coincidence; indeed, scrutiny of the large-Da régime indicates that β there is not $O(\mathrm{Da}^{-1})$, but rather scales inversely with Da ln Da.

https://doi.org/10.1017/S0956792519000238 Published online by Cambridge University Press

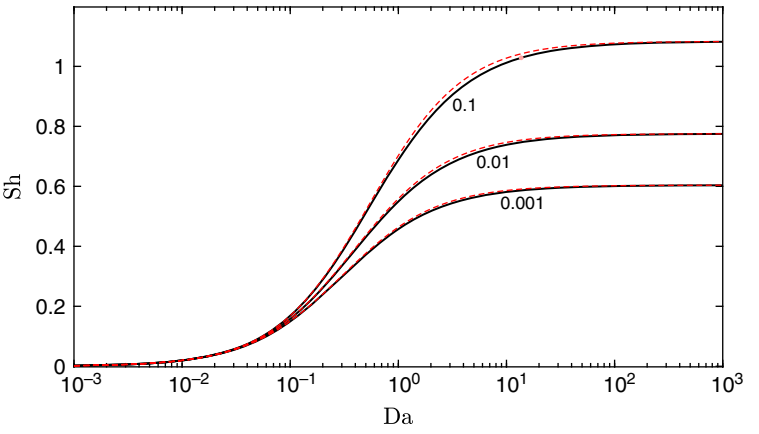

FIGURE 5. Variation of Sh with Da, as obtained from (5.20) , for the indicated values of Pe. Solid: exact solution, with β(Da) determined from (6.11) and (6.13). Dashed: the corresponding small-Da approximation, with β(Da) provided by (6.20).

Nonetheless, the fortuitous resemblance may be exploited to obtain a rough approximation for Sh, as discussed next.

7 Concluding remarks

We conclude by presenting the quantity of interest, namely the Sherwood number, as obtained by substitution into (5.20) of β(Da), the latter calculated by (6.11) and (6.13). The variation of Sh with Da is portrayed in Figure 5 for three (small) values of Pe. At large Da, where $\beta \to 0$, (5.20) is reduced to the transport-limited expression obtained in Ref. [1]. This limit thus corresponds, for a given Pe-value, to the maximal value of Sh. As small Da, Sh diminishes.

Of particular interest is the small-Da limit. As mentioned above, the small-Da approximation (6.20) is fortuitously accurate for the entire practical range of Da-values. (It is a poor approximation for large Da, but then β is vanishingly small anyway.) The associated approximation for Sh, obtained by plugging (6.20) into (5.20), is illustrated in Figure 5. While that approximation is formally valid only for $\mathrm{Da} \ll 1$, it practically applies for all Da. The associated dimensional flux (per unit length) of analytes onto the sensor, associated with that approximation, is

$$\frac{\pi \mathcal{A} D}{\ln(2/\mathrm{Pe}^{1/2}) + \lambda + \pi/2\mathrm{Da}}. \tag{7.1}$$

It may be useful for rule-of-thumb calculations.

An attractive feature of our asymptotic analysis is that the asymptotic correction to (5.20) is algebraically small. This benefit, shared by other small-Péclet-number problems [7], has to do with the underlying linearity. In comparable non-linear problems, notably flows at small Reynolds numbers [10, 15], the non-linearity of the governing equation in the outer region is responsible for generating logarithmically small corrections. 'Algebraically accurate' approximations for these problems thus requires a hybrid approach, where the mathematical problem in the outer region is solved numerically [11]. No such sophisticated methods are needed here.

https://doi.org/10.1017/S0956792519000238 Published online by Cambridge University Press

The 2D model used in the present paper was motivated by the smallness of the sensor length a compared with its width, say w. Given the emergence of an outer region at distances large compared with the sensor length, the mere geometric condition $a \ll w$ is insufficient to justify that model. Indeed, from (3.1) and (5.1), we see that the dimensional extent of the outer region, where diffusive and advective transport are comparable for small Péclet numbers, is of order $\sqrt{D/G}$. The geometric condition should accordingly be refined to $\sqrt{D/G} \ll w$.

Last, consider possible future generalisations. Our analysis makes use of the simplified kinetic condition (3.11), valid at short times. If the exact condition (3.5) were used instead, one could describe the entire time evolution of analyte capture, still within the quasi-steady approximation (3.10). The transport process then consists of two coupled problems. The first governs c via a quasi-steady description; the second, consisting of the evolution equation (3.7) and initial condition (3.8*b*), describes an inherently unsteady problem. This general approach can be implemented by the iteration of two successive steps: in the first, one obtains c for a given distribution of b; in the second, b is marched forward over a small time step using an appropriate numerical scheme. With the need to solve an asymptotic problem (governing c) which depends upon a distribution whose evolution is determined numerically, the above task is quite challenging.

Acknowledgements

I thank Ester Segal and Sofia Arshavsky–Graham for useful discussions.

References

[1] Ackerberg, R. C., Patel, R. D. & Gupta, S. K. (1978) The heat/mass transfer to a finite strip at small Péclet numbers. *J. Fluid Mech.* **86**, 49.
[2] Bender, C. M. & Orszag, S. A. (1978) *Advanced Mathematical Methods for Scientists and Engineers*, McGraw-Hill, New York.
[3] Bretherton, F. P. (1962) Slow viscous motion round a cylinder in a simple shear. *J. Fluid Mech.* **12**, 591.
[4] Bunimovich, Y. L., Shin, Y. S., Yeo, W.-S., Amori, M., Kwong, G. & Heath, J. R. (2006) Quantitative real-time measurements of DNA hybridization with alkylated nonoxidized silicon nanowires in electrolyte solution. *J. Am. Chem. Soc.* **128**, 16323.
[5] Cui, Y., Wei, Q., Park, H. & Lieber, C. M. (2001) Nanowire nanosensors for highly sensitive and selective detection of biological and chemical species. *Science* **293**, 1289.
[6] Ebbens, S., Tu, M.-H., Howse, J. R. & Golestanian, R. (2012) Size dependence of the propulsion velocity for catalytic Janus-sphere swimmers. *Phys. Rev. E* **85**, 020401.
[7] Frankel, N. A. & Acrivos, A. (1968) Heat and mass transfer from small spheres and cylinders freely suspended in shear flow. *Phys. Fluids* **11**, 1913.
[8] Hinch, E. J. (1991) *Perturbation Methods,* Cambridge University Press, Cambridge.
[9] Johnsson, B., Löfås, S. & Lindquist, G. (1991) Immobilization of proteins to a carboxymethyldextran-modified gold surface for biospecific interaction analysis in surface plasmon resonance sensors. *Anal. Biochem.* **198**, 268.
[10] Kaplun, S. (1957) Low Reynolds number flow past a circular cylinder. *J. Math. Mech.* **6**, 595.
[11] Kropinski, M. C. A., Ward, M. J. & Keller, J. B. (1995) A hybrid asymptotic-numerical method for low Reynolds number flows past a cylindrical body. *SIAM J. Appl. Math.* **55**, 1484 (1995).
[12] Leal L. G. (2007) *Advanced Transport Phenomena: Fluid Mechanics and Convective Transport Processes*, Cambridge University Press, New York.
[13] Michelin, S. & Lauga, E. (2014) Phoretic self-propulsion at finite Péclet numbers. *J. Fluid Mech.* **747**, 572.
[14] Moon, P. & Spencer, D. E. (1988) *Field Theory Handbook*. Springer-Verlag, New York.

[15] PROUDMAN, I. & PEARSON, J. R. A. (1957) Expansions at small Reynolds numbers for the flow past a sphere and a circular cylinder. *J. Fluid Mech.* **2**, 237.
[16] SHEEHAN, P. E. & WHITMAN, L. J. (2005) Detection limits for nanoscale biosensors. *Nano Lett.* **5**, 803.
[17] SQUIRES, T. M., MESSINGER, R. J. & MANALIS, S. R. (2008) Making it stick: convection, reaction and diffusion in surface-based biosensors. *Nat. Biotechnol.* **26**, 417.
[18] STERN, E., KLEMIC, J. F., ROUTENBERG, D. A., WYREMBAK, P. N., TURNER-EVANS, D. B., HAMILTON, A. D., LAVAN, D. A., FAHMY, T. M. & REED, M. A. (2007) Label-free immunodetection with CMOS-compatible semiconducting nanowires. *Nature* **445**, 519.
[19] TITCOMBE, M. S. & WARD, M. J. (1997) Convective heat transfer past small cylindrical bodies. *Stud. Appl. Math.* **99**, 81.
[20] VAN DYKE, M. (1964) *Perturbation Methods in Fluid Mechanics*. Academic Press, New York.
[21] YARIV, E. (2016) Wall-induced self-diffusiophoresis of active isotropic colloids. *Phys. Rev. Fluids* **1**, 032101.
[22] ZHENG, G., PATOLSKY, F., CUI, Y., WANG, W. U. & LIEBER, C. M. (2005) Multiplexed electrical detection of cancer markers with nanowire sensor arrays. *Nat. Biotechnol.* **23**, 1294.

Appendix A: Small-X approximation for $C(X, 0)$

Consider the integrand appearing in (5.17). Making use of the large-argument approximation of the Airy function (see [2]), we readily obtain

$$\frac{e^{-i\pi/6}\,\mathrm{Ai}(e^{-i\pi/3}s^{4/3})}{s^{1/3}\,\mathrm{Ai}'(e^{-i\pi/3}s^{4/3})} \sim -\frac{1}{s} \quad \text{for} \quad s \to \infty, \tag{A1}$$

which results, upon the naïve substitution $X = 0$, in an $1/s$ decay rate of the integrand. It follows that the asymptotic evaluation of the integral $I(X)$ for $X \ll 1$ falls under the intermediate case where the dominant contribution is neither local nor global [8]. To evaluate that integral for small X, we split it as

$$\left(\int_0^1 + \int_1^{s^*} + \int_{s^*}^{\infty}\right) \frac{e^{-i\pi/6}\,\mathrm{Ai}(e^{-i\pi/3}s^{4/3})}{s^{1/3}\,\mathrm{Ai}'(e^{-i\pi/3}s^{4/3})} e^{-sX}\,ds \stackrel{\text{def}}{=} I_1 + I_2 + I_3, \tag{A2}$$

wherein we introduce the auxiliary constant s^*. Since that constant is at our disposal, we can choose its value at will; we hereafter restrict it to satisfy $1 \ll s^* \ll 1/X$. In what follows, we consider the limit $X \searrow 0$ and seek the leading-order approximation of I_1, I_2 and I_3. While each of these approximations may generally depend upon s^*, their sum I must be independent of that arbitrary parameter which does not appear in (5.17).

In the evaluation of I_1, we may simply substitute $X = 0$, obtaining

$$I_1 \sim \int_0^1 \frac{e^{-i\pi/6}\,\mathrm{Ai}(e^{-i\pi/3}s^{4/3})}{s^{1/3}\,\mathrm{Ai}'(e^{-i\pi/3}s^{4/3})}\,ds + o(1). \tag{A3}$$

The same is true for I_2, where, following (A1), we further add and subtract $1/s$ from the integrand,

$$I_2 \sim \int_1^{s^*} \left\{\frac{e^{-i\pi/6}\,\mathrm{Ai}(e^{-i\pi/3}s^{4/3})}{s^{1/3}\,\mathrm{Ai}'(e^{-i\pi/3}s^{4/3})} + \frac{1}{s}\right\} ds - \int_1^{s^*} \frac{ds}{s} + o(1). \tag{A4}$$

https://doi.org/10.1017/S0956792519000238 Published online by Cambridge University Press

In view of (A1), the integrand of the first integral decays faster than $1/s$ at large s, thus allowing to replace s^* by ∞ in that integral. This gives

$$I_2 \sim \int_1^\infty \left\{ \frac{e^{-i\pi/6}\,\mathrm{Ai}(e^{-i\pi/3}s^{4/3})}{s^{1/3}\,\mathrm{Ai}'(e^{-i\pi/3}s^{4/3})} + \frac{1}{s} \right\} ds - \ln s^* + o(1). \tag{A5}$$

In evaluating I_3, we cannot substitute $X = 0$, but we can use (A1). This gives $I_3 \sim -\mathrm{E}_1(s^*X)$, wherein E_1 is the exponential integral. Making use of the small-argument expansion of that special function,

$$\mathrm{E}_1(z) \sim -\gamma_\mathrm{E} - \ln z + O(z) \quad \text{for} \quad z \ll 1, \tag{A6}$$

in which γ_E is the Euler–Mascheroni constant, we eventually obtain

$$I_3 \sim \gamma_\mathrm{E} + \ln s^* + \ln X + o(1). \tag{A7}$$

Summing up the three contributions (A3), (A5) and (A7), we find that the $\ln s^*$ terms cancel out whereby the dependence upon s^* disappears, as it should. Substitution into (5.16) and (5.17) eventually furnishes the requisite approximation (5.18), wherein

$$\lambda = -\gamma_\mathrm{E} - \mathrm{Re}\int_0^1 \frac{e^{-i\pi/6}\,\mathrm{Ai}(e^{-i\pi/3}s^{4/3})}{s^{1/3}\,\mathrm{Ai}'(e^{-i\pi/3}s^{4/3})} e^{-sX}\, ds - \mathrm{Re}\int_1^\infty \left\{ \frac{e^{-i\pi/6}\,\mathrm{Ai}(e^{-i\pi/3}s^{4/3})}{s^{1/3}\,\mathrm{Ai}'(e^{-i\pi/3}s^{4/3})} + \frac{1}{s} \right\} ds. \tag{A8}$$

Numerical quadrature of the two integrals appearing in (A8) gives (5.19).

Appendix B: An improved small-Da approximation

Expansion (6.17) is associated with the comparable expansion of β:

$$\beta \sim \frac{\beta_{-1}}{\mathrm{Da}} + \beta_0 + \cdots. \tag{B1}$$

To obtain β_0, we note that $\tilde{c}_0$ satisfies the homogenous conditions (6.7) together with the far-field behaviour (4.5). It accordingly possesses the Fourier-series representation (6.8). The corresponding coefficients $\{A_n\}$ are determined using the condition

$$\frac{\partial \tilde{c}_0}{\partial \eta} = \frac{\sin\psi}{2} \quad \text{at} \quad \eta = 0, \tag{B2}$$

which follows from (6.18) and (6.19) in conjunction with (6.4). We therefore obtain

$$1 - 2\sum\nolimits_{n=0}^{\infty} nA_n \cos 2n\psi = \frac{\pi}{2}\sin\psi. \tag{B3}$$

Multiplying by $\cos 2m\psi$ $(m = 0, 1, \ldots)$ and integrating over ψ in $(0, \pi/2)$ yields

$$mA_m = \delta_{m0} + \frac{1}{4m^2 - 1}, \quad m = 0, 1, \ldots, \tag{B4}$$

where we have used the quadrature

$$\int_0^{\pi/2} \cos 2m\psi \sin\psi\, d\psi = \frac{1}{1 - 4m^2}. \tag{B5}$$

https://doi.org/10.1017/S0956792519000238 Published online by Cambridge University Press

For $m = 0$, (B4) is trivially satisfied, so A_0 remains undetermined. For $m > 0$, we get

$$A_m = \frac{1}{m(4m^2 - 1)}. \tag{B6}$$

To determine A_0, we employ the solvability condition at the next asymptotic order. Thus, consider the $O(\mathrm{Da})$ balance of (6.5*b*),

$$\int_{-1}^{1} \tilde{c}_0|_{\eta=0} \sin\psi \, d\psi = 0. \tag{B7}$$

Substituting (6.8) with (B6) and using again (B5) gives

$$\beta_0 = A_0 = \sum_{m=1}^{\infty} \frac{1}{m(4m^2 - 1)^2} = \frac{3}{2} - \ln 4. \tag{B8}$$

Substitution into (B1) then furnishes (6.21).

https://doi.org/10.1017/S0956792519000238 Published online by Cambridge University Press